Research Article | Vol. 28, No. 25 / 7 December 2020 / Optics Express 37996
Optics EXPRESS

3D-printed optical probes for wafer-level testing of photonic integrated circuits

MAREIKE TRAPPEN,[1,2] MATTHIAS BLAICHER,[1,2] PHILIPP-IMMANUEL DIETRICH,[1,2,3] COLIN DANKWART,[4] YILIN XU,[1,2] TOBIAS HOOSE,[1,2] MUHAMMAD RODLIN BILLAH,[1,2,3] AMIN ABBASI,[5] ROEL BAETS,[5] UTE TROPPENZ,[6] MICHAEL THEURER,[6] KERSTIN WÖRHOFF,[7] MORITZ SEYFRIED,[4] WOLFGANG FREUDE,[1] AND CHRISTIAN KOOS[1,2,3,*]

[1]*Institute of Photonics and Quantum Electronics (IPQ), Karlsruhe Institute of Technology (KIT), Engesserstraße 5, 76131 Karlsruhe, Germany*
[2]*Institute for Microstructure Technology (IMT), Karlsruhe Institute of Technology (KIT), Hermann-von-Helmholtz-Platz 1, 76344 Eggenstein-Leopoldshafen, Germany*
[3]*Vanguard Photonics GmbH, Gablonzer Str. 10, 76185 Karlsruhe, Germany*
[4]*Ficontec Service GmbH, Rehland 8, 28832 Achim, Germany*
[5]*Photonics Research Group, Ghent University – imec, Technologiepark-Zwijnaarde 126, B-9052 Gent, Belgium*
[6]*Fraunhofer Institute for Telecommunications, Heinrich Hertz Institute (HHI), Einsteinufer 37, 10587 Berlin, Germany*
[7]*LioniX International B.V., P.O. Box 456, 7500 AL Enschede, The Netherlands*
[*]*christian.koos@kit.edu*

Abstract: Wafer-level probing of photonic integrated circuits is key to reliable process control and efficient performance assessment in advanced production workflows. In recent years, optical probing of surface-coupled devices such as vertical-cavity lasers, top-illuminated photodiodes, or silicon photonic circuits with surface-emitting grating couplers has seen great progress. In contrast to that, wafer-level probing of edge-emitting devices with hard-to-access vertical facets at the sidewalls of deep-etched dicing trenches still represents a major challenge. In this paper, we address this challenge by introducing a novel concept of optical probes based on 3D-printed freeform coupling elements that fit into deep-etched dicing trenches on the wafer surface. Exploiting the design freedom and the precision of two-photon laser lithography, the coupling elements can be adapted to a wide variety of mode-field sizes. We experimentally demonstrate the viability of the approach by coupling light to edge-emitting waveguides on different integration platforms such as silicon photonics (SiP), silicon nitride (TriPleX), and indium phosphide (InP). Achieving losses down to 1.9 dB per coupling interface, we believe that 3D-printed coupling elements represent a key step towards highly reproducible wafer-level testing of edge-coupled photonic integrated circuits.

1. Introduction

Mass production of photonic integrated circuits (PIC) requires high-throughput wafer-level testing for characterization of device performance early in the fabrication process and prior to entering costly and complex manufacturing steps such as chip separation, anti-reflection coating, and packaging. To this end, light must be efficiently coupled with high reproducibility between in-plane waveguides and single-mode fibers (SMF) oriented in an out-of-plane direction. Presently, optical wafer-level probing of PIC predominantly relies on surface coupling through grating structures [1,2]. However, while grating couplers (GC) have been widely used for silicon-on-insulator (SOI) [2] or silicon nitride (Si_3N_4) [3,4] waveguides, they are not commonly

#405139 https://doi.org/10.1364/OE.405139
Journal © 2020 Received 11 Aug 2020; revised 9 Oct 2020; accepted 14 Oct 2020; published 2 Dec 2020

Optics EXPRESS

available on other platforms such as indium phosphide (InP) or low-index-contrast planar lightwave circuits (PLC). In addition, present PIC designs increasingly rely on edge-coupling (EC), also in the case of silicon photonics [5,6], which offers large transmission bandwidth and permits essentially planar package architectures. The associated waveguide facets are often prepared by deep-etched dicing trenches on the wafer surface and can hence not be accessed with plain SMF. To overcome this problem, PLC-based optical probes with polished 45°-end faces were proposed to couple light from an out-of-plane SMF array to an array of in-plane Si_3N_4 waveguides [7]. However, this approach is limited to rather large mode-field diameters (MFD) of, e. g., 10 µm and leads to comparatively high insertion losses of, e.g., 5.7 dB per coupling interface [7]. Transferring this concept to testing of high index-contrast waveguides with smaller MFD is challenging since the PLC-based probe emits a divergent beam with a diameter larger than 10 µm. Instead of probes on the SMF side, an alternative approach uses redirecting mirrors at the chip side [8]. In this concept, light from a high-index-contrast on-chip waveguide is redirected to a surface-normal direction by means of a metal-coated curved polymer micro-mirror that is fabricated inside the deep-etched dicing trench using gray-tone lithography and e-beam evaporation [8]. With this concept, coupling losses of 3.2 dB have been demonstrated between a high-NA SMF and a tapered silicon photonic (SiP) waveguide. However, the fabrication of the associated metal-coated micromirrors is complicated, costly, and subject to unavoidable structural variations that lead to uncertainties of the optical coupling efficiency and hence obscure the performance of the circuit under test.

In this paper we demonstrate a technically simple and universally applicable approach for low-loss high-throughput optical wafer-level probing of edge-coupled photonic integrated circuits. Our concept relies on 3D-printed freeform micro-optical elements [9] that can be fabricated with high precision on the end faces of standard SMF and that are designed to efficiently couple light to and from waveguide facets at the sidewalls of deep-etched dicing trenches [10]. Each coupling element comprises a total-internal reflection (TIR) mirror for redirecting the light from an out-of-plane to an in-plane direction, followed by an aspheric lens that allows to match the mode field to the respective waveguide type. Exploiting the vast design freedom of 3D-printed freeform optical elements, we design short-focal-distance lenses, which can be used also in narrow trenches. We experimentally demonstrate the viability of our concept by probing Si_3N_4 waveguides (Lionix TriPleX, MFD $D_{\mathrm{WG,TriPleX}} = 10\,\mu\mathrm{m}$), InP-based buried-heterostructure distributed-feedback (DFB) lasers (MFD $D_{\mathrm{WG,InP}} = 3\,\mu\mathrm{m}$), and SiP circuits (MFD $D_{\mathrm{WG,SiP}} = 2.5\,\mu\mathrm{m}$). We achieve coupling losses down to 2.7 dB (TriPleX), 1.9 dB (InP), and 1.9 dB (SiP), respectively. For the silicon photonic chip, we also investigate the reproducibility of the coupling loss for 18 different combinations of waveguide facets and coupling elements, finding a mean value of 2.23 dB and standard deviation of 0.14 dB.

2. Concept

The concept of wafer-level probing with 3D-printed optical coupling elements is illustrated in Fig. 1. The freeform coupling elements are directly printed on the facets of standard SMF arrays, see Fig. 1(a). A planar total-internal reflection (TIR) mirror redirects the beam from an out-of-plane to an in-plane direction, and a freeform aspheric lens is used to match the beam waist diameter at the facet of the on-chip waveguide to the respective mode-field size, Fig. 1(b). The freeform optical coupling elements are designed to transform a beam diameter D_{SMF} at the SMF facet (point S_1) into a diameter D_{WG} at the waveguide facet (point S_4), while fitting into standard dicing trenches of width $w \geq 50\,\mu\mathrm{m}$ and depth $d \geq 20\,\mu\mathrm{m}$. The points S_2 and S_3 denote the intersection point of the beam axis with the TIR mirror and the apex of the aspheric lens, respectively. For efficient coupling, the optical axis (S_2S_3) of the aspheric lens is brought in line with the on-chip waveguide. To prevent mechanical damage while aligning the probe, the distance $H = |\overline{S_1S_2}|$ is chosen sufficiently large, typically in the range (50. . . 130) µm, see

Optics EXPRESS

Fig. 1(b). Note that the divergent beam emitted from the SMF facet propagates freely through the bulk of the 3D-printed coupling element until it reaches the TIR mirror, such that the exact outer shape of the structure along the line $\overline{S_1S_2}$ does not play any role for the optical performance. In our experiments, we tried out different geometries featuring, e.g., an increasing diameter towards the facet of the SMF, Fig. 1(c) and (d), or consisting of more slender structures with constant diameter, Fig. 1(e), which allows to reduce the writing time without any impact on the optical behavior.

For optimizing the refractive surface of the lens, we represent the rotationally symmetric freeform surface by its axial position y as a function of the radial distance r to the optical axis, which we express by an even polynomial with parameters a_{2i}, i=1,...,4,

$$y(r) = \sum_{i=0}^{4} a_{2i} r^{2i} \,, \tag{1}$$

where the radial offset from the optical axis is given by

$$r = \sqrt{x^2 + z^2}. \tag{2}$$

The coordinates x, y, and z used in Eqs. (1) and (2) are defined with respect to a coordinate system having its origin at the intersection point S_2 of the beam axis and the TIR mirror, see inset of Fig. 1(b). The directions of the x, y, and z axis are defined by the coordinate system in the lower left-hand corner of Fig. 1(b). The polynomial parameter $a_0 = |\overline{S_2S_3}|$ hence defines the position of the lens apex along the optical path, whereas the shape of the refracting surface is determined by the parameters a_2, a_4, a_6, and a_8.

For numerical optimization of the lens parameters, we assume a rotationally symmetric Gaussian beam profile having its waist on the SMF end face, where the $1/e^2$ diameter of the intensity distribution amounts to $D_{\mathrm{SMF}} = 10.4\,\mu\mathrm{m}$ [11]. For simplicity, the target field at the chip facet is also approximated by a rotationally symmetric Gaussian with a flat phase front, for which the diameter D_{WG} is adapted to the MFD of the on-chip waveguide. Note that this approach can be extended to, e.g., elliptical mode-field shapes by expanding Eqs. (1) and (2) to non-rotationally-symmetric lens surfaces. For optimizing the lens surface, we fix the propagation length $L = H + a_0$ of the Gaussian beam within the bulk of the coupling element and numerically optimize the parameters a_{2i}, $i = 1 \ldots 4$, for best coupling efficiency under the constraint that a minimum value of $20\,\mu\mathrm{m}$ is maintained for the working distance f to the chip facet, thereby reducing the risk of mechanical damage during alignment of the probe. Note that for a given mode-field diameter of the on-chip waveguide, the requirement of a prescribed minimum working distance f can only be fulfilled if the propagation length L of the weakly diverging Gaussian beam within the bulk of the coupling element is chosen sufficiently large. If L is chosen too small, then the beam diameter in the plane of the aspheric lens is too small, leading to a working distance f below the minimum prescribed value.

If the targeted MFD at the etched waveguide facet exceeds $5\,\mu\mathrm{m}$, we can use a commercial design program (Physical Optics Propagation module of OpticStudio, Zemax [12]) for the lens optimization. For smaller MFD, we exploit a home-made implementation of a wave-propagation algorithm (WPA) that is based on the technique described in [13] and that produces reliable results also for strongly diverging or converging beams. For each optical integration platform, we design a dedicated probe that is geared towards the MFD of the respective on-chip waveguides. Using Gaussian start and target fields, we achieve theoretical coupling efficiencies of 96% (TriPleX, $D_{\mathrm{WG,TriPleX}} = 10\,\mu\mathrm{m}$), 94% (InP, $D_{\mathrm{WG,InP}} = 3\,\mu\mathrm{m}$) and 89% (SiP, $D_{\mathrm{WG,SiP}} = 2.5\,\mu\mathrm{m}$) according to the WPA method, not taking into account Fresnel reflection. Figure 1(c)-(e) shows scanning-electron microscope (SEM) images of the fabricated coupling elements for the TriPleX, the InP, and the SiP platform. Note that even the theoretical coupling efficiencies do not reach

Optics EXPRESS

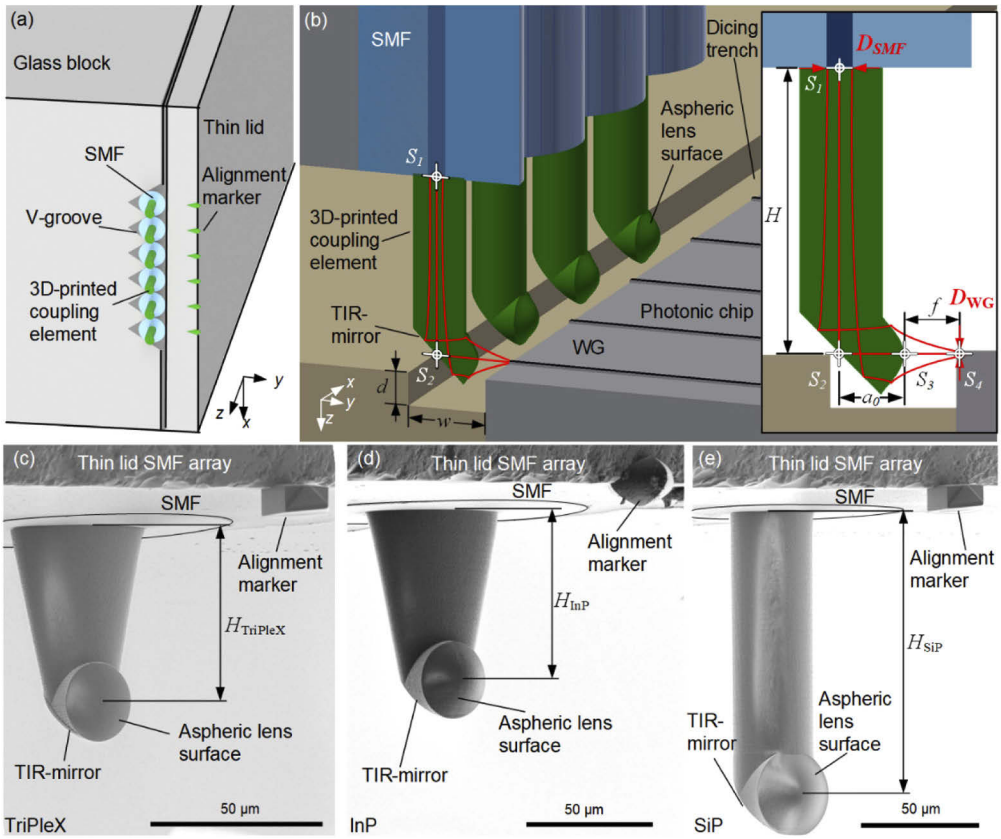

Fig. 1. Concept of wafer-level optical probing with 3D-printed coupling elements. **(a)** Schematic view of 3D-freeform coupling elements (green) printed to the end-face of a single-mode fiber (SMF) array. The SMF array consists of a glass block with V-grooves that hold the fibers and of a thin glass lid. The 3D-printed freeform elements allow for efficient coupling of light between the out-of-plane fibers and in-plane waveguides on the photonic chip. Alignment markers (green) are printed onto the front edge of the lid to facilitate vision-based alignment of the probe with respect to on-chip waveguides, see Fig. 2. **(b)** Close-up view of the optical probe with 3D-printed coupling elements (green) that are inserted into a deep-etched dicing trench (width w, depth d). For illustration, the thin lid as seen in Fig. 1(a) is omitted, and the probe is cut open along the optical axis of the first fiber. Light emitted from the SMF first propagates freely as a Gaussian beam (red) with waist diameter D_{SMF} in the bulk of each coupling element. A total-internal-reflection (TIR) mirror redirects the beam, which is then focused by a freeform aspheric lens to a beam waist diameter D_{WG} that is adapted to the mode-field size of the integrated optical on-chip waveguide at the etched facet. For efficient coupling, the optical axis $\overline{S_2S_3}$ of the aspheric lens is brought in line with the on-chip waveguide. The inset shows a zoom-in of the cut-open coupling element with working distance f, distance a_0 from the TIR mirror, and distance H between the SMF end-face and the optical axis $\overline{S_2S_3}$ of the aspheric lens. **(c)–(d)** Scanning-electron microscope (SEM) images of a single coupling element designed for coupling to **(c)** TriPleX, **(d)** InP and **(e)** SiP waveguides with different distances H. Note that the scale of (c) is different from the scales in (d) and (e)

Optics EXPRESS

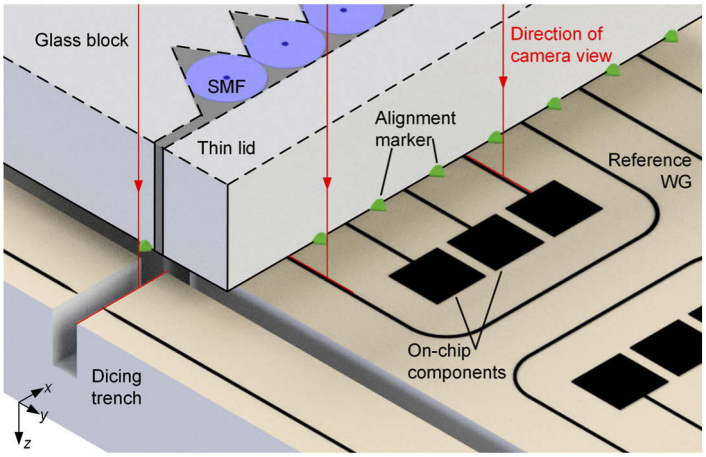

Fig. 2. Coarse alignment of optical probe with respect to on-chip structures by means of 3D-printed alignment markers (green). For illustration, the top of the fiber array is cut away. For coarse positioning in a top-view camera of a wafer prober (viewing direction illustrated by red lines), the markers are aligned with the waveguides on the chip and with the sidewall of the dicing trench that contains the waveguide facets. The coupling efficiency is then optimized by active alignment techniques.

100%. We attribute this to the fact that our system comprises only one freeform surface that is optimized – a single-surface design would be sufficient for Gaussian beams that propagate within the validity range of the paraxial approximation but does not allow to match the amplitude and phase distribution of strongly diverging beams with small spot sizes and non-Gaussian intensity distributions. In the case of the SiP facet, the half-angle of the $1/e^2$ intensity distribution amounts to 22°, which is clearly beyond the 11° limit that is often used to define the validity range of the paraxial approximation [14]. We expect that more complex probe designs with more than one shape-optimized optical surface in combination with more accurate modeling tools and with a more accurate representation of the non-Gaussian waveguide mode field at the facet will allow to further increase the theoretical as well as the experimentally demonstrated efficiencies of our 3D-printed coupling elements.

For testing of integrated waveguide arrays, 3D-printed optical probes can be realized on fiber arrays (FA) with highly accurate pitches of, e. g., 127 µm or 250 µm, see Fig. 2. Probes with smaller pitches of, e.g., 80 µm or 35 µm are also possible by using arrays of thinned SMF [15] or multicore fibers [16] with cores arranged along a line on the fiber end face. 3D-printed alignment markers at the front edge of the FA, see Fig. 1(a) and Fig. 2, can be used as a reference to facilitate vision-based coarse alignment of the coupling elements with respect to on-chip structures in wafer probers with top-view cameras. After coarse alignment in the $(x.y)$-plane, the probe is lowered along z to introduce the coupling elements into the trench, and active alignment techniques are used for refining the optimum coupling position.

To estimate the influence of the alignment precision on the optical coupling efficiency, we simulate the excess coupling loss $10\log_{10}(\eta_m/\eta(r,y))$ as a function of the radial offset $r = \sqrt{x^2+z^2}$ and of the longitudinal offset y from the optimum position with maximum coupling efficiency $\eta_m = \eta(0,0)$. We assume a target waveguide with a Gaussian MFD of $D_{\mathrm{WG,SiP}} = 2.5\,\mu\mathrm{m}$, corresponding to a small silicon photonic (SiP) waveguide, or, alternatively, a waveguide with a Gaussian MFD $D_{\mathrm{WG,TriPleX}} = 10\,\mu\mathrm{m}$ representing a large TriPleX waveguide. The results are shown in Fig. 3. The corresponding working distances, see inset in Fig. 1(b), are $f_{\mathrm{SiP}} = 25\,\mu\mathrm{m}$ and $f_{\mathrm{TriPleX}} = 40\,\mu\mathrm{m}$. The simulated maximum coupling efficiencies amount to $\eta_{m,\mathrm{SiP}} = 0.89$ (0.50 dB

Optics EXPRESS

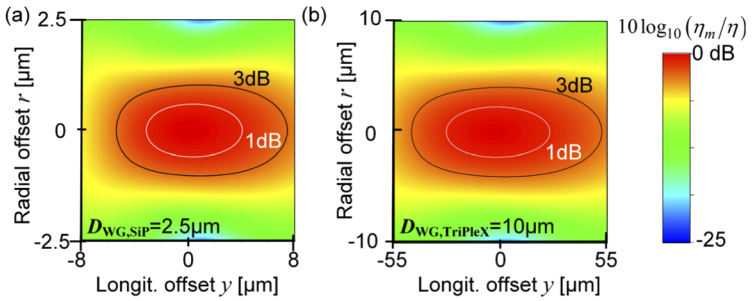

Fig. 3. Analysis of alignment tolerances. The images show the color-coded simulated excess coupling loss $10\log_{10}(\eta_m/\eta(r,y))$ as calculated from the power coupling efficiency $\eta(r,y)$ as a function of radial offset r and longitudinal offset y from the optimum coupling position, for which the maximum coupling efficiency η_m is achieved. The input Gaussian mode field diameter at the end face of the probe fiber is $D_{\mathrm{SMF}} = 10.4\,\mu\mathrm{m}$. **(a)** Coupling to a small silicon photonic (SiP) on-chip waveguide with a mode-field diameter of $D_{\mathrm{WG,SiP}} = 2.5\,\mu\mathrm{m}$ at the facet. The maximum coupling efficiency is $\eta_{\mathrm{m,SiP}} = 0.89$ (0.5 dB loss). The radial 1 dB (3 dB) alignment tolerance amounts to $\pm 0.6\,\mu\mathrm{m}$ ($\pm 1\,\mu\mathrm{m}$), and the longitudinal 1 dB (3 dB) tolerance amounts to $-3\,\mu\mathrm{m}$ / $+4\,\mu\mathrm{m}$ ($-5\,\mu\mathrm{m}$ / $+7\,\mu\mathrm{m}$). **(b)** Coupling to a TriPleX on-chip waveguide with a mode-field diameter of $D_{\mathrm{WG,TriPleX}} = 10\,\mu\mathrm{m}$. The maximum coupling efficiency is $\eta_{\mathrm{m,TriPleX}} = 0.97$ (0.13 dB loss). The radial 1 dB (3 dB) alignment tolerance amounts to $\pm 2.2\,\mu\mathrm{m}$ ($\pm 4.0\,\mu\mathrm{m}$), and the longitudinal 1 dB offset tolerance is $-28\,\mu\mathrm{m}$ / $+25\,\mu\mathrm{m}$ ($-46\,\mu\mathrm{m}$ / $+52\,\mu\mathrm{m}$).

loss) and $\eta_{m,\mathrm{TriPleX}} = 0.97$ (0.13 dB loss) for the silicon photonic and the TriPleX waveguides, respectively. For the target MFD $D_{\mathrm{WG,SiP}} = 2.5\,\mu\mathrm{m}$ of the SiP waveguide, the tolerable radial offset for a 1 dB (3 dB) excess loss amounts to 0.6 µm (1 µm), while the corresponding longitudinal offset tolerance is $-3\,\mu\mathrm{m}$ / $+4\,\mu\mathrm{m}$ ($-5\,\mu\mathrm{m}$ / $+7\,\mu\mathrm{m}$). For the target MFD $D_{\mathrm{WG,TriPleX}} = 10\,\mu\mathrm{m}$ of the TriPleX waveguide, the radial offset tolerance for a 1 dB (3 dB) excess loss is 2.2 µm (4 µm), while the longitudinal offset tolerance is $-28\,\mu\mathrm{m}$ / $+25\,\mu\mathrm{m}$ ($-46\,\mu\mathrm{m}$ / $+52\,\mu\mathrm{m}$). The required precision for active alignment complies well with the typical positioning step size of 100 nm that is specified for commercially available optical probing systems [17,18]. Note that, for probing of integrated waveguide arrays, not only the positioning accuracy of the alignment stage, but also the pitch accuracy of the optical probes and the fabrication tolerances of the 3D-printed elements may contribute to excess coupling loss. Since the coupling elements are precisely aligned to the respective fiber cores during the fabrication process, their pitch accuracy is mainly dictated by that of the underlying fiber array, which shows typical variations of $\pm 0.3\,\mu\mathrm{m}$ [19]. This effect is discussed in more detail in Section 4.

3. Fabrication

The coupling elements are printed on the facets of standard SMF arrays using a customized two-photon lithography system (Nanoscribe Photonic Professional GT, 40× objective with NA = 1.4), which was complemented by a proprietary control software. The 3D structure is built up by writing consecutive lines on different layers into a negative-tone photoresist. In our experiments, both the writing distance between lines (hatching) and the spacing of layers (slicing) are set to 100 nm for generating smooth reflective and refractive surfaces of TIR mirrors and lenses. The core of each SMF is automatically detected, and the coupling element and its associated alignment marker are written in a single write field for avoiding stitching errors. Similar processes have previously been used for fabrication of 3D freeform waveguides for

Optics EXPRESS

chip-chip connections, so called photonic wire bonds [20,21], or for 3D printing of optically actuated scanning-probe microscopy (SPM) engines [22].

Figure 1(c), (d), and (e) shows SEM images of optical coupling elements designed for SiP, InP, and TriPleX waveguides. For the coupling element designed for SiP waveguides, the beam needs to be focused to a fairly small MFD $D_{WG,SiP} = 2.5\,\mu m$. This requires a high numerical aperture (NA), which, in combination with the working distance of $f_{SiP} = 25\,\mu m$, leads to a rather large beam diameter of 23 µm in a cross-sectional plane at the lens apex S_3. For a given waist diameter D_{SMF} at the SMF surface, the beam diameter at the lens dictates the propagation distance of the beam within the bulk of the coupling element, which amounts to $L_{SiP} = H_{SiP} + a_{0,SiP} = 164\,\mu m$ for the SiP design. For coupling elements designed for the TriPleX waveguides, the targeted MFD of $D_{WG,TriPleX} = 10\,\mu m$ is larger, and the propagation distance in the coupling element can thus be reduced to $L_{TriPleX} = H_{TriPleX} + a_{0,TripLeX} = 90\,\mu m$. While a larger MFD D_{WG} at the facet of the on-chip waveguide can reduce the required total length L of the coupling element for a given value of D_{SMF}, another possible solution is to reduce the working distance f to achieve smaller beam diameters on the lens surface. For coupling to the small MFD $D_{WG,InP} = 3\,\mu m$ of an InP waveguide, a working distance of $f_{InP} = 20\,\mu m$ is chosen, which reduces the geometrical propagation distance in the coupling element to $L_{InP} = H_{InP} + a_{0,InP} = 95\,\mu m$. The diameter of the coupling elements is chosen to provide sufficient room for the divergent beam that is emitted from the SMF and that freely propagates through the bulk of the 3D-printed coupling element.

4. Experimental verification

To demonstrate the viability of our concept, we perform coupling experiments to integrated edge-emitting waveguides realized on three different platforms, namely Si_3N_4 waveguides (Lionix TriPleX) with a targeted MFD of $D_{WG,TriPleX} = 10\,\mu m$ at the facet, InP-based DFB lasers ($D_{WG,InP} = 3\,\mu m$), and SiP circuits ($D_{WG,SiP} = 2.5\,\mu m$). Due to the lack of full wafers, we performed these measurements on diced chips that were equipped with facets in deep-etched trenches. However, due to the compactness of the probes, this should not represent a fundamental difference to on-chip probing. For alignment of the coupling elements with respect to the waveguide facets, we use a pair of six-axes positioning stages and manually optimize for best coupling efficiency.

For coupling to TriPleX [23] waveguides with rather large MFD of $D_{WG,TriPleX} = 10\,\mu m$, we use a loop-back waveguide with 250 µm spacing between the edge couplers. Incoupling and outcoupling of light with a wavelength of 1550 nm is accomplished through different coupling elements on a common fiber array see Fig. 4(a). The measured loss per coupling is 2.7 dB, which can be considered as a conservative estimate since we assumed lossless on-chip waveguides in this case. As a reference, we also couple light from the 3D-printed coupling element to the facet of an SMF with an MFD of 10.4 µm, which leads to a coupling loss of only 1.6 dB and to a measured 1 dB lateral alignment tolerance of ± 2.3 µm, in good agreement with simulations, see Fig. 3(b). We attribute the slightly higher coupling loss in the chip-probing experiment to the significant roughness of the TriPleX chip facet. Still, the measured coupling loss is much smaller than the 5.7 dB that were previously demonstrated for coupling between on-chip Si_3N_4 waveguides and PLC-based optical probes with polished 45° end faces [7]. In this context, it is important to note that our 3D-printed coupling elements focus light to a point at a working distance $f = 40\,\mu m$ away from the lens apex. The associated focal spot can be moved even beyond the chip edge for the case that the tip of the on-chip waveguide is slightly retracted from sidewall of the deep-etched dicing trench. In contrast to our arrangement, the waist of an optical beam emitted by a PLC-based probe is always within the probe or at its facet, which needs to be brought in close proximity to the waveguide end face, thus bearing the risk of damaging the probe and/or the chip edge.

Optics EXPRESS

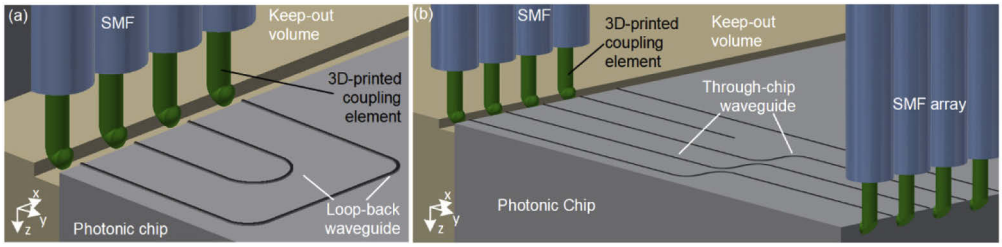

Fig. 4. Artist's impression of setup for optical probing with 3D-printed coupling elements. **(a)** Measurement of loop-back waveguides: For optimum coupling, the position and orientation of the SMF array with the 3D-printed coupling elements is adjusted in six degrees of freedom, comprising translation along and rotation about each of the x-, y-, and z-axis. For better visibility, the cover lid of the fiber arrays is omitted. **(b)** Coupling to through-chip waveguides using a pair of probes with 3D-printed coupling elements: Each of the probes is aligned in six degrees of freedom. For better visibility, the glass blocks of the fiber arrays are omitted.

For coupling experiments with integrated InP waveguides, we use buried-heterostructure DFB lasers (Fraunhofer HHI) emitting at a wavelength of 1590 nm with an MFD of 3 µm measured at the device facet [9]. As a reference, we first measured the power emitted from the DFB laser as a function of the pump current (*P-I*-curve) using an integrating sphere which was brought into close proximity of the laser facet. The *P-I*-curve was again measured through the 3D-printed coupling element after optimizing the position of the probe with respect to the laser facet. As a reference point for the coupling loss, we choose a pump current of 50 mA, for which the laser is specified. Compared to the power measured by the integrating sphere, we estimate a loss of 1.9 dB for the 3D-printed coupling element.

For coupling to SiP circuits at 1550 nm, we rely on test chips fabricated on the standard silicon photonics platform of Interuniversity Microelectronics Centre (IMEC), Belgium, having edge couplers with a measured MFD of 2.5 µm. We explore both coupling to loop-back waveguides with 250 µm, 1250 µm and 1750µm spacing between the edge couplers, where incoupling and outcoupling of light is accomplished through different coupling elements on a common fiber array, Fig. 4(a), and coupling to through-chip waveguides with a pair of independently movable probes, Fig. 4(b). For each configuration, we perform a series of measurements using different combinations of on-chip waveguides and 3D-printed coupling elements. In each of these measurements, the probe position and orientation is individually optimized to achieve maximum transmission. The losses of 0.17 dB/mm of the on-chip waveguides are extracted from measured reference structures and taken into account when estimating the coupling losses. For through-chip waveguides, we find a coupling loss of (2.23 ± 0.14) dB per interface, extracted from 18 measurements. For the loop-back waveguides, the measured coupling loss amounts to (2.43 ± 0.35) dB, extracted from 17 measurements with waveguides of different spacings between the edge couplers. The smallest measured loss per coupling interface is 1.9 dB. Note that the average coupling loss for the loopback structures is only slightly higher than that obtained for the through-chip waveguides. This indicates that inaccuracies of the probe pitch or other fabrication-related variations of the 3D-printed coupling elements do not play a significant role.

We further investigate the impact of probe-pitch inaccuracy, which may become a prominent impairment when probing arrays of regularly spaced SiP waveguides with small mode-field diameters ($D_{\mathrm{WG,SiP}} = 2.5$ µm). To this end, we use an SMF array with eight 3D-printed elements that are simultaneously coupled to four on-chip loop-back waveguides. In a first step, we optimize the position and the orientation of the SMF array by maximizing the transmission through a reference channel comprising the first and the last coupling element along with the outermost

Optics EXPRESS

loopback structure, see Fig. 4(a) for an illustration of an array-probing experiment with only four coupling elements. We then translate the SMF array in the x- and the z-direction, i.e., transverse to the optical axis of the on-chip waveguide, and record the transmission through all four channels, each comprising an on-chip loopback waveguide along with the associated pair of coupling elements. The position-dependent transmission η_{LB} of each of the four loopback channels is fitted by a Gaussian with variable position, peak coupling efficiency, and $1/e^2$-width. We then extract the (x, z)-position of the maximum of each of these Gaussians, corresponding to the optimum probe position for the respective channel. We find that the optimum z-positions of the probe are very similar for the various channels, with a standard deviation of only $\sigma_{\mathrm{pr},z} \approx 0.08\,\mu\mathrm{m}$, whereas the optimum x-positions exhibit a stronger variation with a standard deviation of $\sigma_{\mathrm{pr},x} \approx 0.28\,\mu\mathrm{m}$. This variation of the optimum coupling positions can be translated into a position variation of the associated coupling elements and the associated focal spots produced on the waveguide facet. In general, both the coupling element at the input and at the output facet will be subject to position inaccuracy, which can be expressed by transverse offsets $\Delta x_{\mathrm{i}},\ \Delta z_{\mathrm{i}}$ at the input and $\Delta x_{\mathrm{o}},\ \Delta z_{\mathrm{o}}$ at the output coupling element. Optimum transmission through the channel as a whole is achieved for an 'intermediate' transverse offset of the fiber probe, for which the coupling elements at the input and the output facet have an offset with respect to the optimum position. The optimum transverse offset of the probe is hence given by the average of the transverse offsets of the two coupling elements, $\Delta x_{\mathrm{pr}} \approx (\Delta x_{\mathrm{i}} + \Delta x_{\mathrm{o}})/2$ and $\Delta z_{\mathrm{pr}} \approx (\Delta z_{\mathrm{i}} + \Delta z_{\mathrm{o}})/2$. Assuming identical Gaussian distributions for Δx_{i} and Δx_{o} with variances $\overline{\Delta x_{\mathrm{i}}^2} = \overline{\Delta x_{\mathrm{o}}^2} = \sigma_{\mathrm{ce},x}^2$, where the overbar denotes an expectation value, we can express the variance of the probe position Δx_{pr} in the horizontal direction by $\overline{\Delta x_{\mathrm{pr}}^2} = \sigma_{\mathrm{pr},x}^2 = \sigma_{\mathrm{ce},x}^2/2$. Similarly, the variance of the probe position Δz_{pr} in the vertical direction is given by $\overline{\Delta z_{\mathrm{pr}}^2} = \sigma_{\mathrm{pr},z}^2 = \sigma_{\mathrm{ce},z}^2/2$. From the measured standard deviations $\sigma_{\mathrm{pr},x} \approx 0.28\,\mu\mathrm{m}$ and $\sigma_{\mathrm{pr},z} \approx 0.08\,\mu\mathrm{m}$ of the optimum probe position, we may hence estimate the variances of the focal spot position of the coupling elements to be $\sigma_{\mathrm{ce},x} \approx 0.40\,\mu\mathrm{m}$ and $\sigma_{\mathrm{ce},z} \approx 0.11\,\mu\mathrm{m}$. This is in line with the expectation that the laser lithography is fairly accurate, leading to a small offset of the focal spot along z, whereas the positioning accuracy of the coupling elements along x is limited by the inaccurate pitch of the fiber array, for which a typical variation of $\pm 0.3\,\mu\mathrm{m}$ is specified by the manufacturer [19].

Based on these findings we may now estimate the excess coupling loss associated with the pitch inaccuracy of the underlying fiber probe. To this end, we first consider the simulated dependence of the efficiency η of a single coupling interface on the transverse misalignment in Fig. 3(a), and we describe this relationship by a Gaussian. Exploiting the fact that a transverse misalignment Δx and Δz of the focal spot of a coupling element with respect to the axis of the on-chip waveguide leads to a radial offset $r = \sqrt{\Delta x^2 + \Delta z^2}$ and taking into account that coupling of two identical Gaussian mode fields with identical variances $(D_{\mathrm{WG,SiP}}/2)^2$ leads to a position-dependence of the coupling efficiency with variance $\sigma_\eta^2 = 2(D_{\mathrm{WG,SiP}}/2)^2 = D_{\mathrm{WG,SiP}}^2/2$, this Gaussian can be written as

$$\eta(\Delta x, \Delta z) = \eta_{\mathrm{m}} \exp\left(-\frac{\Delta x^2 + \Delta z^2}{2{\sigma_\eta}^2}\right), \tag{3}$$

where $\sigma_\eta = 1.77\ \mu\mathrm{m}$ is obtained for $D_{\mathrm{WG,SiP}} = 2.5\ \mu\mathrm{m}$. This relation may be translated into a dB-value for the coupling loss,

$$\eta_{\mathrm{dB}}(\Delta x, \Delta z) = 10\log_{10}\left(\frac{\eta_{\mathrm{m}}}{\eta(\Delta x, \Delta z)}\right) \approx 4.34 \times \frac{\Delta x^2 + \Delta z^2}{2{\sigma_\eta}^2}. \tag{4}$$

To quantify the excess loss η_{dB}, we next estimate the transverse misalignment Δx and Δz of the focal spot of a coupling element with respect to the facet of the corresponding on-chip waveguide in the array-probing scenario. To this end, we first need to account for the fact that the fiber probe is initially aligned based on an inaccurately positioned pair of coupling elements for the

Optics EXPRESS

reference channel. In this alignment step, the optimum coupling efficiency is again reached when the probe is adjusted to an 'intermediate' position given by Δx_{pr} and Δz_{pr}, for which the two coupling elements at the input and the output facet have the same offset with respect to the optimum position. For given variances $\overline{\Delta x_{\mathrm{ce}}^2} = \sigma_{\mathrm{ce},x}^2$ and $\overline{\Delta z_{\mathrm{ce}}^2} = \sigma_{\mathrm{ce},z}^2$ of the focal-spot positions of the coupling elements in the reference channel, the variance of the probe position is again given by $\overline{\Delta x_{\mathrm{pr}}^2} = \sigma_{\mathrm{pr},x}^2 = \sigma_{\mathrm{ce},x}^2/2$ and $\overline{\Delta z_{\mathrm{pr}}^2} = \sigma_{\mathrm{pr},z}^2 = \sigma_{\mathrm{ce},z}^2/2$. Besides the incorrectly positioned probes, the efficiency of a certain coupling interface of interest is impaired by the transverse offsets Δx_{ce} and Δz_{ce} of the associated coupling elements. The total transverse offsets of the focal spot with respect to the optical axis of the on-chip waveguide hence amount to $\Delta x = \Delta x_{\mathrm{pr}} + \Delta x_{\mathrm{ce}}$ and $\Delta z = \Delta z_{\mathrm{pr}} + \Delta z_{\mathrm{ce}}$. Assuming that all positioning inaccuracies are statistically independent, the variances of the associated errors may be added, $\overline{\Delta x^2} \approx \overline{\Delta x_{\mathrm{pr}}^2} + \overline{\Delta x_{\mathrm{ce}}^2} = 3\sigma_{\mathrm{ce},x}^2/2$ and $\overline{\Delta z^2} \approx \overline{\Delta z_{\mathrm{pr}}^2} + \overline{\Delta z_{\mathrm{ce}}^2} = 3\sigma_{\mathrm{ce},z}^2/2$. With Eq. (4), the expectation value of the excess loss induced by position inaccuracy of the various coupling elements can thus be written as

$$\bar{\eta}_{\mathrm{dB}} \approx 4.34 \times \frac{3(\sigma_{\mathrm{ce},x}^2 + \sigma_{\mathrm{ce},z}^2)}{4{\sigma_\eta}^2}. \tag{5}$$

Inserting the values $\sigma_{\mathrm{ce},x} \approx 0.40\,\mu\mathrm{m}$, $\sigma_{\mathrm{ce},z} \approx 0.11\,\mu\mathrm{m}$, and $\sigma_\eta = 1.76\ \mu\mathrm{m}$, we find that the additional loss due to alignment inaccuracy of the 3D-printed coupling elements is approximately 0.18 dB. Note that this analysis is based on a rather small statistical base of only eight coupling elements and four transmission channels that were investigated in our experiment. Still, it may give an approximate quantitative indication of the effects of pitch inaccuracy of the 3D-printed coupling elements, based on which we believe that the inaccuracies of fiber pitch are not a fundamental limitation, even for probing of SiP waveguide arrays with small cross sections.

It should be noted that the above-mentioned coupling loss of 1.9 dB measured for SiP waveguides deviates clearly from the simulated loss of 0.50 dB. The excess loss found in the experiment can be attributed to several effects. First, all our measurements rely on manual optimization of the position and the orientation of the probe in six degrees of freedom. Each of these optimizations required several iterations, since the Pivot point of the positioning stage did not coincide with the focal spot of the coupling element. We expect that fully automated active alignment procedures with proper Pivot-point calibration might further reduce the coupling losses and improve the reproducibility, especially for coupling to waveguide arrays as demonstrated for the SiP loop-back waveguides. Second, our simulations and optimizations of the optical coupling elements rely on the assumption of an ideal Gaussian beam, which does only approximately reflect the true beam shape. In addition, this simulation does not account for the reflection of 4% at the lens-air interface. Third, surface roughness due to discrete printing layers leads to scattering loss, both at the TIR mirror and at the lens surface. Moreover, additional losses can be caused by imperfections of the fabrication process: Laser power fluctuations may lead to a deviation of the refractive index or of the position of the lens surface from its target value, and unwanted shrinkage may further impair the geometry of the structure. Both effects influence the shape of the emitted beam and thereby the measured coupling efficiency. Hence, while our proof-of-concept experiments demonstrate the versatility and performance of 3D-printed coupling elements for wafer-level probing, we expect that further improvements of the coupling efficiency can be achieved by optimized design, fabrication and positioning of the coupling elements. Note that, due to the strong curvature of the lens surface, the Fresnel reflection due to the refractive-index difference does not necessarily lead to excessive unwanted back-reflection of light into the probed waveguide – even in absence of an AR coating. Properly designed 3D-printed coupling elements may hence also be suitable for probing of devices that are sensitive to spurious back reflection such as semiconductor optical amplifiers (SOA).

Optics EXPRESS

5. Summary

We have introduced and experimentally demonstrated a novel approach for optical wafer-level probing of edge-coupled photonic integrated circuits (PIC). The concept relies on compact 3D-printed coupling elements, which can be inserted into standard dicing trenches etched into the wafer surface. Exploiting the design freedom and the precision of two-photon laser lithography, the coupling elements can be adapted to a wide variety of mode-field sizes. In our experiments, we demonstrate losses down to 2.7 dB, 1.9 dB, and 1.9 dB when coupling to silicon-nitride (TriPleX, $D_{\mathrm{WG,TriPleX}} = 10\,\mu\mathrm{m}$) on-chip waveguides, InP-based active optical components (InP, $D_{\mathrm{WG,InP}} = 3\,\mu\mathrm{m}$) and silicon photonic (SiP, $D_{\mathrm{WG,SiP}} = 2.5\,\mu\mathrm{m}$) on-chip waveguides, respectively. The technique is well suited for parallel probing of multiple optical ports through arrays of single-mode fibers, each of which is equipped with a dedicated coupling element. We believe that 3D-printed optical probes have the potential to revolutionize wafer-level testing of advanced photonic integrated circuits.

Funding

Deutsche Forschungsgemeinschaft (EXC-2082/1-390761711, 1173); Bundesministerium für Bildung und Forschung (13N14630); European Research Council (773248); Horizon 2020 Framework Programme (731954); Helmholtz International Research School for Teratronics, Karlsruher Institut für Technologie; Karlsruhe School of Optics and Photonics; Karlsruhe Nano-Micro Facility (KNMF).

Acknowledgments

This work was supported by the Deutsche Forschungsgemeinschaft (DFG, German Research Foundation) under Germany's Excellence Strategy via the Excellence Cluster 3D Matter Made to Order (EXC-2082/1-390761711) as well as through the Collaborative Research Centre (CRC) WavePhenomena (# 1173), by the Bundesministerium für Bildung und Forschung (BMBF) via the joint project PRIMA (13N14630), by the European Research Council (ERC Consolidator Grant 'TeraSHAPE', # 773248), by the H2020 Photonic Packaging Pilot Line PIXAPP (# 731954), by the Helmholtz International Research School for Teratronics (HIRST), by the Karlsruhe School of Optics and Photonics (KSOP), and by the Karlsruhe Nano-Micro Facility (KNMF).

Disclosures

P.I.D. and C.K. are co-founders and shareholders and M.R.B. is an employee of Vanguard Photonics GmbH and Vanguard Automation GmbH, start-up companies engaged in exploiting 3D nanoprinting in the field of photonic integration and assembly. C.D. and M.S. are employees of ficonTEC GmbH, a company engaged in developing and selling optical assembly and test equipment. M.T, M.B. and T.H. have recently been employed by Nanoscribe GmbH, a company developing 3D printing tools as used in this publication. M.T, P.-I.D., M.B., T.H., M.R.B., Y.X., and C.K. are co-inventors of patents owned by Karlsruhe Institute of Technology (KIT) in the technical field of the publication.

References

1. D. Thomson, A. Zilkie, J. E. Bowers, T. Komljenovic, G. T. Reed, L. Vivien, D. Marris-Morini, E. Cassan, L. Virot, J.-M. Fédéli, J.-M. Hartmann, J. H. Schmid, D.-X. Xu, F. Boeuf, P. O'Brien, G. Z. Mashanovich, and M. Nedeljkovic, "Roadmap on silicon photonics," J. Opt. **18**(7), 073003 (2016).
2. D. Taillaert, P. Bienstman, and R. Baets, "Compact efficient broadband grating coupler for silicon-on-insulator waveguides," Opt. Lett. **29**(23), 2749–2751 (2004).
3. G. Maire, L. Vivien, G. Sattler, A. Kaźmierczak, B. Sanchez, K. B. Gylfason, A. Griol, D. Marris-Morini, E. Cassan, D. Giannone, H. Sohlström, and D. Hill, "High efficiency silicon nitride surface grating couplers," Opt. Express **16**(1), 328–333 (2008).

Optics EXPRESS

4. J. Hong, A. M. Spring, F. Qiu, and S. Yokoyama, "A high efficiency silicon nitride waveguide grating coupler with a multilayer bottom reflector," Sci. Rep. **9**(1), 12988 (2019).
5. R. Marchetti, C. Lacava, L. Carroll, K. Gradkowski, and P. Minzioni, "Coupling strategies for silicon photonics integrated chips," Photonics Res. **7**(2), 201–239 (2019).
6. C. Kopp, S. Bernabé, B. B. Bakir, J.-M. Fedeli, R. Orobtchouk, F. Schrank, H. Porte, L. Zimmermann, and T. Tekin, "Silicon Photonic Circuits: On-CMOS Integration, Fiber Optical Coupling, and Packaging," IEEE J. Sel. Top. Quantum Electron. **17**(3), 498–509 (2011).
7. R. Polster, L. Y. Dai, O. A. Jimenez, Q. Cheng, M. Lipson, and K. Bergman, "Wafer-scale high-density edge coupling for high throughput testing of silicon photonics," in *Optical Fiber Communication Conference, OSA Technical Digest* (Optical Society of America, 2018), paper M3F.2.
8. A. Noriki, T. Amano, D. Shimura, Y. Onawa, H. Yaegashi, H. Sasaki, and M. Mori, "45-degree curved micro-mirror for vertical optical I/O of silicon photonics chip," Opt. Express **27**(14), 19749–19757 (2019).
9. P.-I. Dietrich, M. Blaicher, I. Reuter, M. Billah, T. Hoose, A. Hofmann, C. Caer, R. Dangel, B. Offrein, U. Troppenz, M. Moehrle, W. Freude, and C. Koos, "In situ 3D nanoprinting of free-form coupling elements for hybrid photonic integration," Nat. Photonics **12**(4), 241–247 (2018).
10. M. Trappen, M. Blaicher, P.-I. Dietrich, T. Hoose, Y. Xu, M. R. Billah, W. Freude, and C. Koos, "3D-Printed Optics for Wafer-Scale Probing," *2018 European Conference on Optical Communication (ECOC)*, Rome, (2018), paper Tu4C.2.
11. Corning, **"**Corning® SMF-28® ultra optical fiber," https://www.corning.com/media/worldwide/coc/documents/Fiber/SMF-28%20Ultra.pdf.
12. Zemax LLC, **"**OpticStudio," https://www.zemax.com/products/opticstudio.
13. S. Schmidt, T. Tiess, S. Schröter, R. Hambach, M. Jäger, H. Bartelt, A. Tünnermann, and H. Gross, "Wave-optical modeling beyond the thin-element-approximation," Opt. Express **24**(26), 30188–30200 (2016).
14. G. Wencker, **"**Ein Beitrag zur Theorie Gaußscher Strahlen (On the theory of Gaussian beams)", Doctoral dissertation thesis (Techn. Hochschule Aachen, 1968) (in German).
15. Corning, **"**Corning® RC SMF Specialty Optical Fibers," https://www.corning.com/microsites/coc/oem/documents/specialty-fiber/RC-SMF.PDF.
16. Fibercore, **"**Multicore Fiber," https://www.fibercore.com/product/multicore-fiber.
17. FiconTEC, **"**TL2000Opto-electronics Chip Tester," https://www.ficontec.com/wp-content/uploads/pdf/TestLine-TL2000-1603en.pdf.
18. MPI Corporation, **"**SiPH Upgrade| 200 and 300 mm Automated Probe SystemsThe Dedicated Solution for Silicon Photonics Device Characterisation," https://www.mpi-corporation.com/wp-content/uploads/ASTPDF/MPI-SiPH-Automated-Probe-Systems-Upgrade-Data-Sheet.pdf
19. SQS-Fiberoptics, "V-Grooves and Fiber Arrays," https://www.sqs-fiberoptics.com/images/pdf-soubory/v-grooves-fiber-optic-arrays.pdf
20. M. Blaicher, M. R. Billah, J. Kemal, T. Hoose, P. Marin-Palomo, A. Hofmann, Y. Kutuvantavida, C. Kieninger, P.-I. Dietrich, M. Lauermann, S. Wolf, U. Troppenz, M. Moehrle, F. Merget, S. Skacel, J. Witzens, S. Randel, W. Freude, and C. Koos, "Hybrid multi-chip assembly of optical communication engines by in situ 3D nano-lithography," Light: Sci. Appl. **9**(1), 71 (2020).
21. M. R. Billah, M. Blaicher, T. Hoose, P.-I. Dietrich, P. Marin-Palomo, N. Lindenmann, A. Nesic, A. Hofmann, U. Troppenz, M. Moehrle, S. Randel, W. Freude, and C. Koos, "Hybrid integration of silicon photonics circuits and InP lasers by photonic wire bonding," Optica **5**(7), 876–883 (2018).
22. P.-I. Dietrich, G. Göring, M. Trappen, M. Blaicher, W. Freude, T. Schimmel, H. Hölscher, and C. Koos, "3D-Printed Scanning-Probe Microscopes with Integrated Optical Actuation and Read-Out," Small **16**(2), 1904695 (2020).
23. K. Wörhoff, R. G. Heideman, A. Leinse, and M. Hoekman, "TriPleX: a versatile dielectric photonic platform," Adv. Opt. Technol. **4**(2), 189–207 (2015).